Boundary mixing in the thermocline of a large lake

Andreas Lorke[1]

Received 9 November 2006; revised 11 April 2007; accepted 11 June 2007; published 21 September 2007.

[1] High-resolution measurements of near-bottom temperature stratification and current velocity were performed on the sloping boundary of a large lake at the depth of the seasonal thermocline. The measurements cover nearly the entire stratified period and reveal the periodic occurrence of strong temperature and current velocity fluctuations, which can be attributed to shoaling high-frequency internal waves with periods between 5 and 20 min. Two different techniques are applied to obtain a long-term record of dissipation rates of turbulent kinetic energy from the current velocity measurements. Shoaling of high-frequency internal waves is associated with a strong and rapid increase of turbulent dissipation rates of up to four orders of magnitude. Since the occurrence of high-frequency internal waves on the slope is correlated with the passage of the dominant basin-scale internal Kelvin wave with a period of four days, energy dissipation rates on the slope vary with the same period. Diapycnal diffusivities, estimated by combining the dissipation estimates with simultaneously measured density stratification, follow a similar dynamics and a comparison with a basin-scale diffusivity estimate based on tracer measurements reveal the importance of boundary mixing, which, at this particular site, is mainly driven by the interaction of high-frequency internal waves with the sloping boundary.

Citation: Lorke, A. (2007), Boundary mixing in the thermocline of a large lake, *J. Geophys. Res.*, *112*, C09019, doi:10.1029/2006JC004008.

1. Introduction

[2] The role of propagating high-frequency internal waves for the transfer of energy from long internal waves to boundary mixing on slopes received increasing attention within the past decades [*Imberger*, 1998; *Wüest and Lorke*, 2003; *Wunsch and Ferrari*, 2004]. Critical reflection of internal waves from sloping bottom topography was observed by *Eriksen* [1982, 1998] and was studied theoretically (*Thorpe* [1999] provided a recent review). The production of turbulence by breaking internal waves on slopes and hence their potential contribution to boundary mixing processes was studied in the laboratory [*Boegman et al.*, 2005a; *Helfrich*, 1992; *Ivey and Nokes*, 1989] as well as numerically [*Javam et al.*, 1999; *Slinn and Riley*, 1996] and enhanced turbulence near boundaries is frequently observed in lakes [*Hondzo and Haider*, 2004; *MacIntyre et al.*, 1999] as well as in the ocean [*Ledwell et al.*, 2000; *Moum et al.*, 2002; *Rudnick et al.*, 2003]. The sparse spatial and temporal resolution of turbulence measurements in the field, which are usually performed using profiling or towed instrument packages, however, do not allow to highlight the contribution of internal wave breaking to the enhanced bottom boundary layer turbulence. Most estimates of the energy flux from internal waves to mixing on sloping boundaries are based on energetic considerations applied to observed internal wave properties [*Boegman et al.*, 2005a; *Eriksen*, 1985]. This rather indirect approach is limited by simplifications of the characteristics of the internal wavefield and of its interaction with the sloping boundary (e.g., linear wave theory or the neglect of wave-wave interactions).

[3] Recent technological advances [*Lorke and Wüest*, 2005; *Wiles et al.*, 2006] allow for an estimation of turbulence dissipation rates from moored acoustic Doppler current profiler (ADCP) measurements, enabling quasi-continuous and long-term observations of dissipation profiles. In this paper we analyze a long-time data set from the sloping boundary of a large lake and present direct measurements of turbulence associated with the shoaling and breaking of high-frequency internal waves at the depth of the thermocline. Dissipation rates of turbulent kinetic energy are estimated from two acoustic current meters using the inertial dissipation and the structure function technique. The latter technique, in particular, allows for dissipation rate estimates with a temporal resolution of 1 min and hence provides a suitable technique to observe the dynamics of turbulence generated by breaking internal waves.

[4] Experimental details and analysis techniques are described in section 2 below. Within the results section we discuss the dynamics of observed temperature and current velocity (3.1) and the dynamics of turbulence dissipation rates (3.2), before we take advantage of the long-term record of turbulence dissipation, current shear and stratification and discuss various aspects of small-scale turbulence and mixing (3.3). A brief discussion of our results in terms

[1]Environmental Physics, Limnological Institute, University of Konstanz, Konstanz, Germany.

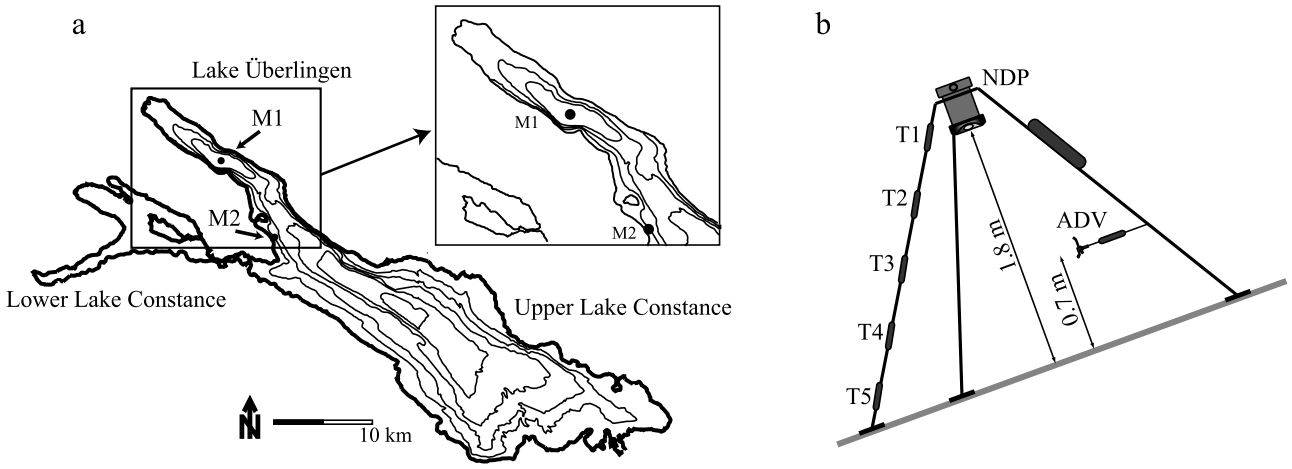

Figure 1. (a) Map of Lake Constance (47°83′99N, 9°81′89E) and location of the moorings M1 and M2. The contour lines represent isobaths with an increment of 50 m. M2 was deployed about 75 m offshore at a depth of 11 m. (b) Details of mooring M2, showing the mounting of the Doppler current profiler (NDP), the Doppler velocimeter (ADV) and the 5 thermistors (T1–T5). M2 was deployed on a steep slope (figure is not to scale) and the deployment heights of the current meters are indicated.

of flux paths of energy in stratified waters is provided in section 4.

2. Materials and Methods

2.1. Measurements

[5] Lake Constance (Figure 1a) is one of the largest lakes in Central Europe. The lake consists of two basins connected by the shallow Lake Rhine: the deep main basin Upper Lake Constance (63 km long, 14 km wide) is located upstream of the shallower basin, called Lower Lake Constance. The central part of Upper Lake Constance has a maximum depth of 252 m and a mean depth of 101 m. Its sub-basin Lake Überlingen (maximum and mean depths are 147 m and 84 m, respectively) is separated from the central part of Upper Lake Constance by the Mainau Sill reaching up to 100 m water depth. For general information on the hydrodynamics of Upper Lake Constance see *Bäuerle et al.* [1998].

[6] This study concentrates on data from two different moorings deployed in Upper Lake Constance: Mooring M1, located at 147 m depth in the deepest part of Lake Überlingen (Figure 1a), measures meteorological parameters at the lake surface and water temperature at 34 depth levels using a fast-response thermistor chain (Precision Measurement Engineering, Inc., USA) at a sampling interval of 60 s. The mooring has been operated continuously since December 2003.

[7] Mooring M2 was deployed on a steep slope (approximately 35°), about 75 m offshore, near the intersection of Lake Ueberlingen and the central basin of Upper Lake Constance (Figure 1a). It consists of a Doppler current profiler (NDP, Nortek AS, Norway), an acoustic Doppler velocimeter (Vector ADV, Nortek AS, Norway), and five individual temperature loggers (TR-1050, RBR Ltd., Canada). The instruments were mounted on a two meter high tripod, which was deployed at a depth of 11 m (Figure 1b). The 1.5 MHz NDP was mounted downward looking on the top of the tripod. It was operated in pulse-coherent mode, resolving velocity profiles between ~0.03 and 1.71 m above the sediment surface with a vertical resolution of 0.03 m. Ten individual profiles were averaged internally before the data were recorded every 10 s. The ADV was mounted horizontally in the center of slanted NDP beams at a height of 0.7 m above the sediment (Figure 1b). It measured the 3-dimensional velocity within a cylindrical sampling volume of 15 × 14.9 mm, at a distance of 0.15 m from the probe at a sampling frequency of 16 Hz. The NDP and the ADV were connected to an onshore power supply and computer for online data recording. Near-bottom temperature stratification was measured using the five temperature loggers at heights of 1.69, 1.35, 1.0, 0.67, and 0.32 m above the sediment at a sampling frequency of 0.1 Hz. Mooring M2 was operated from 7 July to 12 November 2005.

2.2. Data Analysis

[8] Current velocities measured by the ADV and by the NDP were rotated horizontally to represent cross-shore, along-shore, and vertical (normal to the local sediment surface) velocity components, respectively. Vertical shear of both horizontal (bottom parallel) velocity components was estimated by linear regression over 10 adjacent NDP depth cells (0.3 m).

[9] Three different estimates of dissipation rates ε of turbulent kinetic energy were obtained from the measurements at mooring M2: The inertial dissipation technique was applied to the ADV ($\varepsilon_{\mathrm{ADV}}$) and to the NDP ($\varepsilon_{\mathrm{NDP}}$) data, and, in addition, the structure function technique was applied to the NDP data ($\varepsilon_{\mathrm{SF}}$). The inertial dissipation technique is based on fitting velocity fluctuation spectra in the wave number domain Φ_i to the universal Kolmogorov spectrum:

$$\Phi_i = \alpha_i \varepsilon^{2/3} k_i^{-5/3}$$

The index i refers to the along-stream (i = 1) and cross-stream (i = 2, 3) components of the wave number spectrum,

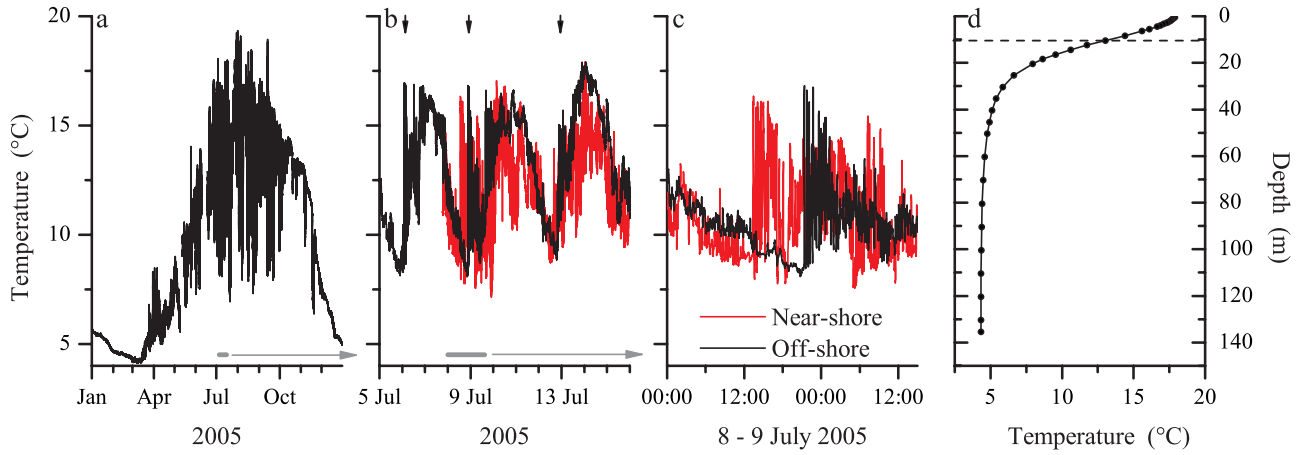

Figure 2. (a) Time series of temperature measured at 10 m depth at the offshore mooring M1. (b) Same as panel (a) with an expanded time axis, emphasizing the basin-scale Kelvin wave. The red line shows the temperature measured at 10 m depth at the nearshore mooring M2 and the arrows on top indicate high-frequency internal wave events. The grey bars in panels (a) and (b) show the span of the time axis in panels (b) and (c), respectively. (c) Same as panel (b), with a further expanded time axis, emphasizing the passage of high-frequency internal waves. (d) Temperature profile measured at mooring M1, averaged over the time period depicted in panel (b). The dashed line indicates the depth of the measurements shown in panels (a) to (c).

k is the wave number, and α_i refers to the one-dimensional Kolmogorov constant α_K ($\alpha_1 = \alpha_K$, $\alpha_2 = \alpha_3 = 4/3\alpha_K$) with $\alpha_K = 1.56$. By applying Taylor's hypothesis Φ_i is calculated from measured time series of the three-dimensional velocity, and ε is estimated by spectral fitting [*Dewey and Crawford*, 1988; *McPhee*, 1998; *Stips*, 2005]. The inertial dissipation technique cannot be applied to three-dimensional current velocities in orthogonal coordinates measured by acoustic Doppler current profilers because such instruments average the velocities over horizontal scales which are typically larger than the relevant turbulent length scales. *Lorke and Wüest* [2005], however, have demonstrated that the inertial dissipation technique can be applied to the in-beam velocity fluctuations measured by Doppler current profilers. Since such instruments cannot resolve the direction of the turbulent in-beam velocity fluctuations, application of the inertial dissipation technique results in an uncertainty of an unknown isotropy constant α_i [*Lorke and Wüest*, 2005]. Dissipation rates estimated from the NDP were calculated using the isotropy constant α_K and hence represent upper limits for ε. Velocity spectra were estimated for half-overlapping segments of 128 data points (NDP) and 4096, 16.384 and 65.536 data points (ADV), respectively. The resulting spectral averaging intervals are 21 min for the NDP and 4, 17, and 68 min for the ADV. The respective dissipation estimates from the three different NDP beams and from the three spectral fits for the ADV were averaged logarithmically [*Baker and Gibson*, 1987].

[10] Application of the structure function technique to current velocity measurements using an acoustic Doppler profiler was recently described by *Wiles et al.* [2006]. Here the spatial correlation of in-beam current velocities is used to estimate dissipation rates ε_{SF}:

$$D(z,r) = C_\nu^2 \varepsilon_{SF}^{2/3} r^{2/3}$$

where $D(z, r) = \overline{(u(z) - u(z+r))^2}$ is the correlation function of in-beam current velocities u as a function of depth z and separation distance r, and $C_\nu^2 \approx 2.1$ is an empirical constant. As for the inertial dissipation technique, ε_{SF} is estimated by fitting the measured correlation functions, which were estimated using the centered difference scheme described by *Wiles et al.* [2006], to the above equation. We used a maximum separation distance of six adjacent NDP bins (0.06 m $\leq r \leq$ 0.18 m) and we averaged the correlation functions of 6 and 128 individual velocity profiles (i.e., 1 and 21 min averaging interval) prior to estimating ε_{SF}. The dissipation rate estimates from the three different NDP beams were averaged logarithmically.

3. Results

3.1. Stratification and Forcing

[11] Lake Constance is a monomictic lake, performing deep convective mixing during winter (December–March) and developing a strong seasonal thermocline during summer (June–October). The seasonal temperature dynamics at 10 m depth is shown in Figure 2a. A pronounced feature, besides the seasonal cycle of temperature, is the strong temperature variance during the stratified season. The dynamics of temperature fluctuations at different timescales is depicted in greater detail in Figures 2b and 2c. A prominent feature of Lake Constance is a basin-scale vertical mode-one Kelvin wave with a period of approximately 4 days [*Appt et al.*, 2004; *Bäuerle et al.*, 1998] with typical thermocline displacements of 5–10 m. The temperature fluctuations associated with the passage of the Kelvin wave do not show great differences in phase and amplitude between the two moorings (Figure 2b). The crests of the Kelvin wave (temperature minima in Figure 2b) are followed by packets of high-frequency internal waves with periods of 5–20 min (Figure 1c) and with amplitudes which are comparable to or even can exceed those of the Kelvin

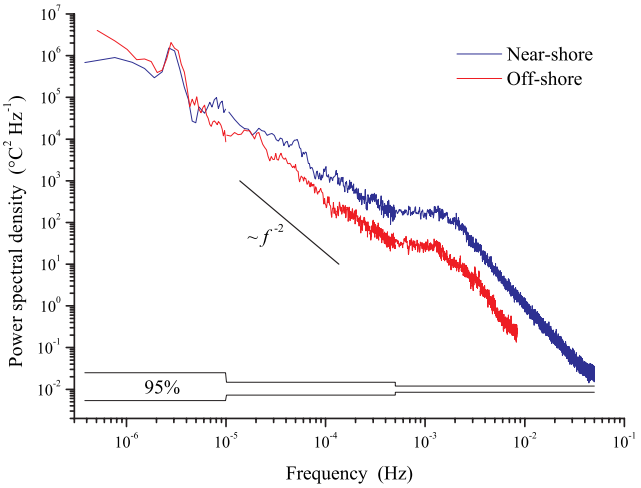

Figure 3. Power spectra of temperature fluctuations measured at 10 m depth at the nearshore and at the offshore mooring. The composite spectra were estimated for the time period from 24 June to 23 October 2005. Frequencies are in cyclic units and the 95% confidence interval of power spectral density is indicated.

wave. Figure 2d shows the typical summer stratification of the offshore water column, averaged over several Kelvin wave periods. Maximum buoyancy frequencies within the thermocline are typically 0.01 Hz (40 cycles per hour, cph) but can reach maximum values of 0.02 Hz (70 cph), whereas the depth of the maximum buoyancy frequency varies between 2 and 20 m.

[12] The correlation between the passage of the basin-scale Kelvin wave and the observation of high-frequency internal waves at the boundary of the Lake Constance is discussed in greater detail in *Lorke et al.* [2006].

[13] A comparison of temperature spectra estimated at 10 m depth at both mooring sites is shown in Figure 3. The spectral distributions of temperature fluctuations at the nearshore and at the offshore moorings are remarkably similar and compare very well to the spectra measured by *Appt et al.* [2004] at a variety of offshore stations in Lake Constance. Both spectra show a peak of comparable amplitude at a frequency around $3{\cdot}10^{-6}$ Hz, corresponding to a period of about 93 h, which can be attributed to the basin-scale Kelvin wave. At higher frequencies, the spectral power declines proportional to frequency squared. The most significant difference between the nearshore and the offshore measurements can be found at frequencies between $5{\cdot}10^{-4}$ and $1.5{\cdot}10^{-3}$ Hz, where both spectra exhibit a plateau with elevated spectral power in comparison to the $\sim f^{-2}$ slope. Here the spectral power in the nearshore data exceeds the power found in the offshore data by a factor of about 6. As discussed in *Lorke et al.* [2006] this frequency range is dominated by high-frequency internal waves.

[14] Current velocities at M2 at 10 m depth vary between $O(10^{-2})$ m s^{-1} up to 0.1–0.2 m·s^{-1} (Figure 4a). No signal of the basin-scale Kelvin wave can be found in the current velocity spectra [*Lorke et al.*, 2006], but high-frequency internal waves are a major source of variance for the cross-shore and vertical velocity components in particular (Figure 4b). This is most obvious by comparing the velocity variance in Figure 4a during the stratified and the non-stratified period. Strong current velocities, which are mainly associated with high-frequency internal waves, are parallel to the bottom.

3.2. Dissipation Rates

3.2.1. Statistics

[15] Dissipation rates ε of turbulent kinetic energy are estimated from the current velocity measurements of the two different instruments using two different methods and varying averaging intervals. For a comparison of these different estimates we consider here the frequency distributions of the total data sets. All observed dissipation rate distributions were fitted to a lognormal distribution ($r^2 > 0.98$), which is used to estimate mean dissipation rates and variances (Table 1). Selected frequency distributions are shown in Figure 5. The mean values of the fitted lognormal distributions of the entire data sets are, with two exceptions, between 5.6 and $7.1{\cdot}10^{-8}$ W·kg^{-1}. The two exceptions are the dissipation estimates from the NDP using the structure function technique and an averaging interval of 1 minute, and the dissipation estimates from the NDP using the inertial dissipation technique with an averaging interval

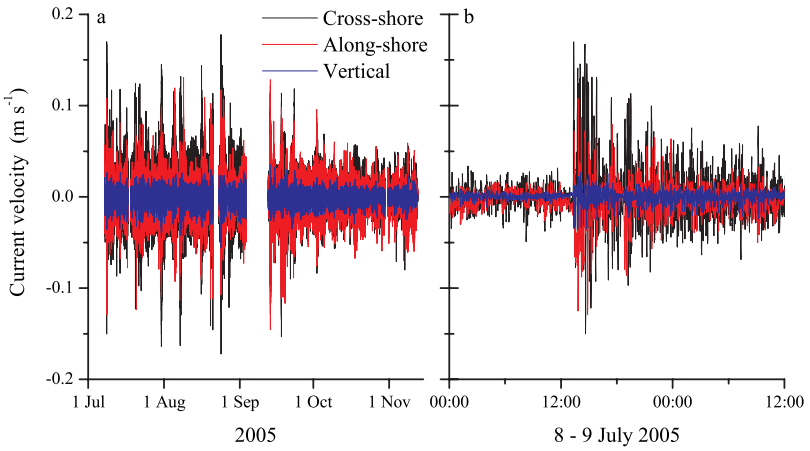

Figure 4. (a) Current velocity measured at the nearshore mooring M2 at a height of 0.7 m above the sediment by the NDP. (b) Same as (a), emphasizing a high-frequency internal wave event (see Figure 2c for associated temperature fluctuations).

Table 1. Average Values ($\langle\varepsilon\rangle$) and Variances ($\sigma^2$) of Dissipation Rate Estimates Using Different Methods and Different Averaging Intervals[a]

Instrument - Method	Averaging Interval (No. of Data Points)	No. of Observations	$\langle\varepsilon\rangle$, W kg^{-1}	σ^2 (W kg^{-1})^2
NDP - structure function	21 min (128)	16.161	$7.1\cdot10^{-8}$	1.0
NDP - structure function	1 min (6)	322.625	$2.9\cdot10^{-8}$	2.2
NDP - inertial dissipation	21 min (128)	16.161	$2.8\cdot10^{-8}$	1.0
ADV - inertial dissipation	68 min (65536)	5.664	$6.2\cdot10^{-8}$	0.8
ADV - inertial dissipation	17 min (16384)	23.888	$5.6\cdot10^{-8}$	1.0
ADV - inertial dissipation	4 min (4096)	96.769	$5.9\cdot10^{-8}$	1.4

[a]The averaging interval is given in minutes and in number of data points used for individual dissipaton estimates. Average values were estimated by fitting a lognormal distribution to the entire distribution of dissipation rate estimates (cf. Figure 5).

of 21 min. Both mean values are around $3\cdot10^{-8}$ W·kg^{-1} (Table 1). A close agreement between the mean values of the frequency distributions of the same variable sampled with different temporal resolutions can only be expected if the underlying statistical distribution is stationary. Although, the observed distributions could be fitted to lognormal distributions, it is very unlikely that the long-term record of dissipation rate estimates follows a lognormal distribution, which is a valid approach for homogenous turbulence only [*Yamazaki and Lueck*, 1990]. Indeed, the frequency distribution of the dissipation rate estimates from the ADV using the short spectral averaging interval of 4 min is significantly skewed toward smaller dissipation rates (Figure 5). There seem to be no systematic differences between the dissipation rates estimated from the two different instruments or by applying the two different techniques and the major influence on the actual dissipation estimate is due to the amount of temporal averaging.

3.2.2. Dynamics

[16] Time series of two selected dissipation rate estimates are shown in Figure 6. These particular dissipation rate estimates were chosen because they (i) are based on measurements from two different instruments (ADV vs. NDP), (ii) were obtained using different methods (inertial dissipation vs. structure function technique), and (iii) involve very different scales of temporal averaging (1 min vs. 1 h). The variation of the one minute-based dissipation rate estimates spans seven orders of magnitude from 10^{-11} to 10^{-4} W·kg^{-1} (Figure 6a). In accordance with the frequency distributions shown in Figure 5, the variation is reduced to four orders of magnitude (10^{-8} to 10^{-4} W·kg^{-1}) for the dissipation rates estimated using the inertial dissipation technique and a spectral averaging interval of 68 min, indicating that considerable variance occurs on timescales of less than one hour. Application of a running average on the short-term dissipation rate estimates in Figure 6a results in an almost perfect match of the two dissipation rate time series.

[17] The temporal dynamics of dissipation rates during the internal wave event depicted in Figure 2d (temperature) and in Figure 4b (current velocity) is shown in Figure 6b. With the arrival of the high-frequency internal waves at the sampling site, the dissipation rates "jump" from $\varepsilon \sim 10^{-9}$ W·kg^{-1} to $\varepsilon \sim 10^{-5}$ W·kg^{-1} and recover slowly afterward. This saw tooth like dynamics is typical for most internal wave events observed and the spikes indicating high dissipation rates during summer in Figure 6a are all associated with shoaling high-frequency internal waves. Further evidence for the periodic occurrence of high dissipation rates is provided by the dissipation rate spectra (Figure 7), which show a broad peak around a frequency of $3\cdot10^{-6}$ Hz and a corresponding period of about 4 days. For higher frequencies f, the spectral variance declines proportional to $f^{-0.9}$. Similar to the spectra of temperature fluctuations (Figure 3), the dissipation spectra show a plateau within the internal wave frequency band, before the spectral variance declines rapidly toward higher frequencies. The almost perfect agreement of the spectra of the two different dissipation estimates (Figure 7, cf. also Figure 6) indicates that both estimates have the same temporal dynamics at frequencies $\leq 2\cdot10^{-4}$ Hz and hence provides further confidence in the two different estimation techniques.

[18] Similar to the long-term temperature (Figure 2a) and current velocity (Figure 4a) records, the dissipation rates seem to show a seasonal pattern with enhanced variance and maximum dissipation rates during the stratified season.

3.2.3. Vertical Structure

[19] The vertical structure of current velocities and dissipation rates during the passage of an internal wave is exemplified in Figure 8. Both parameters do not show a pronounced vertical structure and the actual boundary layer is restricted to 0.2 to 0.3 m above the sediment surface. Neither the current velocities nor the dissipation rates show

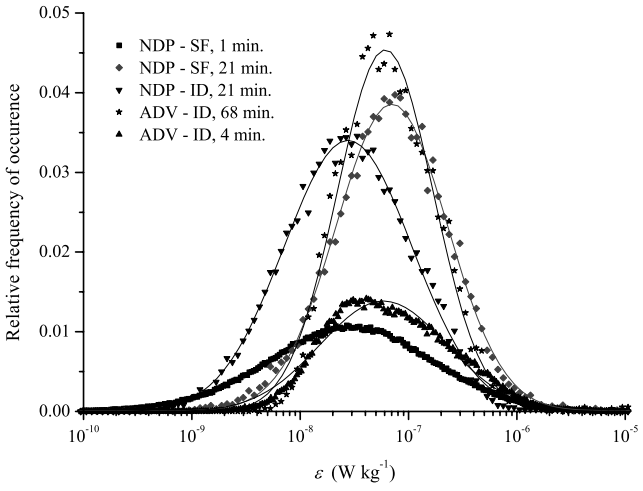

Figure 5. Frequency distributions of dissipation rate estimates using different methods (SF – structure function method, ID – inertial dissipation method) and different averaging intervals. Data points represent the observed distributions based on the entire data set and lines show a fit to a lognormal distribution (see Table 1 for the resulting fit parameters). The distributions are normalized by the total number of observations. Note that the frequency distributions are estimated for $\log_{10}(\varepsilon)$ on a logarithmic bin size distribution.

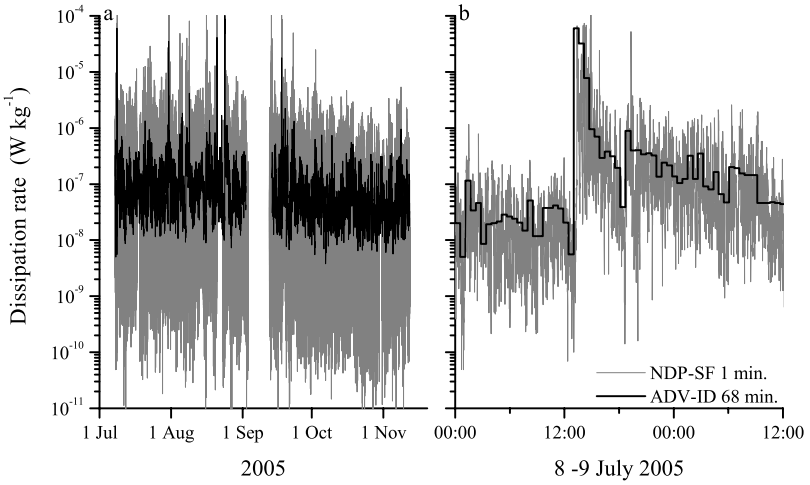

Figure 6. (a) Time series of dissipation rates of turbulent kinetic energy at mooring M2. The dissipation rates are estimated from the NDP data using the structure function method with an averaging interval of 1 minute (NDP-SF, 1 min) and from the ADV data using the inertial dissipation method and an averaging interval of 68 min (ADV-ID, 68 min), respectively. (b) Same as (a), emphasizing a high-frequency internal wave event (see Figures 2c and 4b for associated temperature and current velocity fluctuations).

law-of-the-wall characteristics (logarithmic velocity and reciprocal dissipation rate distribution as a function of distance from the bottom) within this thin layer. Besides measurement and processing limitations in the vicinity of the sediment surface, the observed deviations from law-of-the-wall behavior can be attributed to the non-stationarity and oscillatory nature of the flow [*Lorke et al.*, 2002; *Mellor*, 2002].

[20] As demonstrated in Figure 8, the enhanced dissipation rates during internal wave events measured at a height of 0.7 m above the sediment (deployment height of the ADV), which are discussed above, are not the result of local bed shear stress and can hence be attributed to wave breaking. The latter conclusion is further supported by the fact that the dissipation rates measured 0.7 m above the sediment within an individual wave (Figure 8b) are rather constant and are not correlated with the magnitude of the current velocity.

3.3. Small-Scale Turbulence and Mixing

3.3.1. Production vs. Dissipation

[21] The complete turbulent kinetic energy ($TKE = {}^1/_2\overline{u_i'u_i'}$) budget reads [*Ivey and Imberger*, 1991]:

$$-\frac{\partial}{\partial t}\left(\frac{\overline{u_i'u_i'}}{2}\right)-\overline{u_j}\frac{\partial}{\partial x}\left(\frac{\overline{u_i'u_i'}}{2}\right)-\frac{\partial}{\partial x_j}\left(\frac{1}{\rho_0}\overline{u_j'p'}\right)$$
$$-\frac{\partial}{\partial x_j}\left(\overline{u_j'u_i'u_i'}\right)-\overline{u_i'u_j'}\frac{\partial \overline{u_i}}{\partial x_j}=\frac{g}{\rho_0}\overline{u_3'\rho'}+\varepsilon$$

i.e., $m = m_1 + m_2 + m_3 + m_4 + m_5 = J_b + \varepsilon$ where x_j are the coordinate axes with direction 3 vertically upward, J_b is the buoyancy flux (change of potential energy due to mixing), ε is the rate if viscous dissipation of TKE and m denotes the rate of change of TKE. The total rate of change of locally available mechanical energy is composed of the rate of change of TKE (m_1), advection of TKE by the mean flow (m_2), pressure gradient work (m_3), transport of TKE by turbulent velocity fluctuations (m_4), and local production of TKE (shear production, m_5).

[22] Common assumptions to most applications of the TKE budget equation to naturally occurring turbulent flows are stationarity and homogeneity, which lead to a simplified balance between shear production, buoyancy flux and dissipation [*Gregg*, 1980; *Ivey and Imberger*, 1991; *Osborn*, 1980]. It can be further assumed that the buoyancy flux consumes only a small fraction of the produced TKE (at most 15 to 25 %, [*Osborn*, 1980]) so that a close equilibrium between production and dissipation of TKE can be expected.

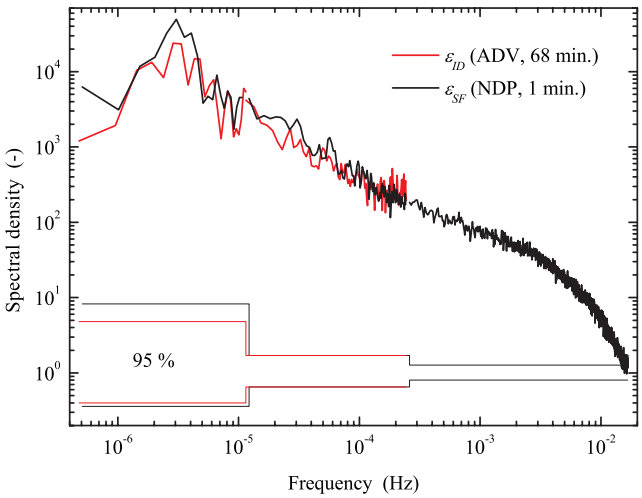

Figure 7. Composite dissipation rate spectra. The spectra are calculated for $\log_{10}(\varepsilon)$, for the dissipation rates estimated between 7 July and 2 September using the inertial dissipation technique applied to segments of 65.536 ADV samples (ε_{ID}, red line) and using the structure function method averaged over 6 individual NDP profiles (ε_{SF}, black line, cf. Table 1). Frequencies are in cyclic units and the respective 95% confidence intervals are indicated.

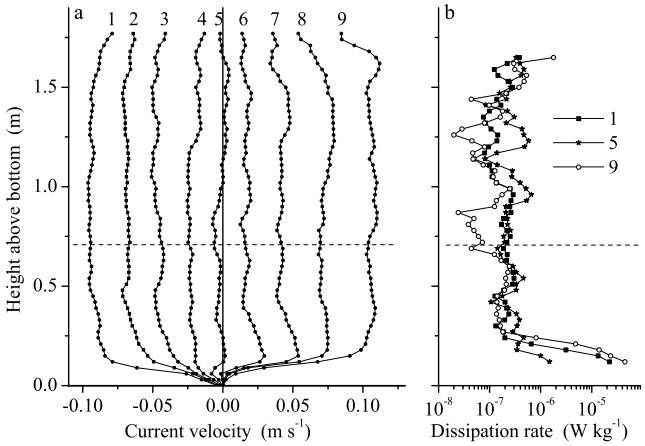

Figure 8. (a) Vertical profiles of the cross-shore current velocity during the passage of an internal wave. The profiles were measured on 8 July 2005 between 14:39:30 (profile 1) and 14:43:30 (profile 9) and numbers refer to subsequent profiles with a time increment of 30 s. Panel (b) shows the respective vertical profiles of dissipation rates for profiles 1,5 and 9. The dashed line indicates the deployment height of the ADV and the vertical measuring position of the current velocity and dissipation rate time series shown in Figures 4 and 6, respectively.

[23] Shear production was estimated using Reynolds stresses ($\overline{u_1' u_3'}$ and $\overline{u_2' u_3'}$) from the ADV and vertical velocity shear ($\frac{\partial u_1}{\partial x_3}$ and $\frac{\partial u_2}{\partial x_3}$) measured by the NDP. Figure 9 shows production rates of TKE versus dissipation rates (ε_{SF}). The estimated production rates are positive as well as negative with a frequency distribution, which is almost symmetrical around zero. Figure 9 shows production versus dissipation rates for the entire data set. Although there is a clear correlation between both rates, the scatter, particularly at low dissipation rates, covers several orders of magnitude, suggesting that a local equilibrium between production and dissipation of TKE is not a valid assumption.

[24] The TKE production (term m_5) is formed by the product of the vertical momentum flux (Reynolds' stress) with the vertical velocity gradient. Positive TKE production rates indicate an up-gradient momentum flux or a transfer of energy from turbulence to the mean flow. Within individual eddies the instantaneous momentum flux is both ways (up- and down-gradient). An eddy carries higher momentum down-gradient, but, if the momentum is not fully mixed within the first half of the eddy's turnover period, it carries also part of the higher momentum back, up-gradient. The normalized difference $(F_{down} - F_{up})/F_{down}$ between the down- (F_{down}) and up-gradient (F_{up}) momentum flux can be interpreted as a mixing efficiency for momentum. On

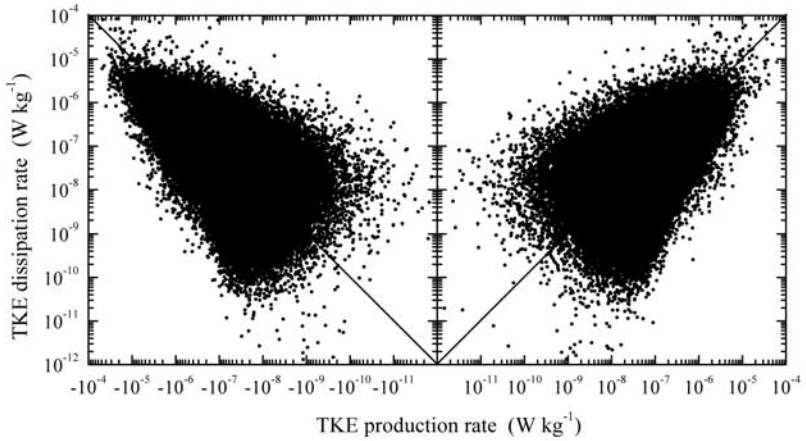

Figure 9. Dissipation rates versus Production rates of turbulent kinetic energy based on one minute estimates. Whereas the dissipation rates were estimated from the NDP data using the structure function method, production rates were estimated by combining Reynolds stress measurements from the ADV with velocity shear measurements from the NDP. The left panel shows negative and the right panel positive production rates. The lines indicate a 1:1 relationship.

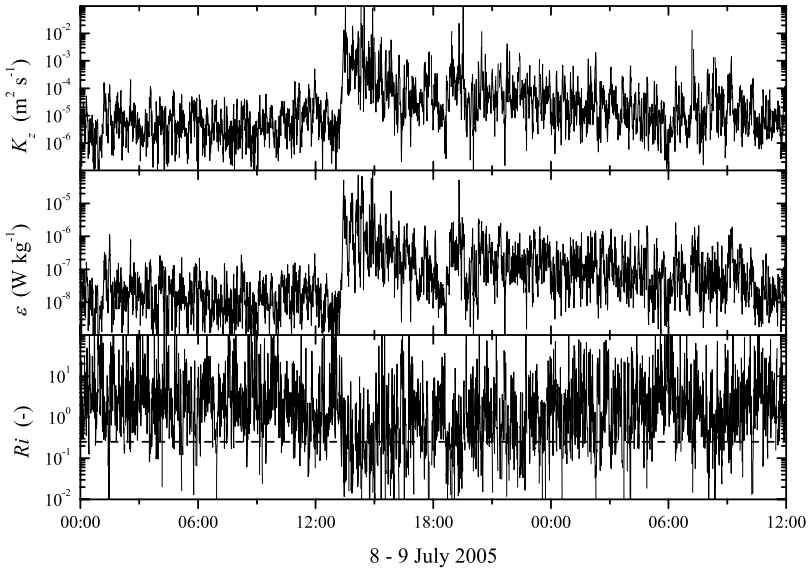

Figure 10. Time series of the gradient Richardson number Ri (lower panel), the dissipation rates of TKE ε (center), and of the diapycnal diffusivities K_z (upper panel) for the internal wave event already depicted in Figures 2c, 4b, and 6b. The dashed line in the lower panel indicates the critical Richardson number Ri_c. The depicted sample resolution is one minute.

average (indicated by an overbar in the TKE equation) the net momentum flux should be down-gradient and the production term m_5 should hence be negative. The averaging process, however, is problematic if the turbulence is not stationary [*Winters et al.*, 1995]. On one hand, at least during time periods when shoaling high-frequency internal waves are the major source for TKE production, stationarity can only be expected on timescales which are short compared to the internal wave periods. On the other hand, the averaging timescale should be large compared to typical eddy turnover periods in order to capture their statistical properties. The production and dissipation rates shown in Figure 9 were estimated over one minute sampling intervals. Within internal wave events like the one exemplified in Figure 6b, the production rates fluctuate between positive and negative values on these short timescales.

[25] It should be noted that our coordinate system is not aligned strictly vertically, but is vertically with respect to the sediment surface (Figure 1b). This choice was taken because the current velocities are mainly in parallel and current shear can be expected to be mainly normal to the bottom. Since we did not measure buoyancy fluxes, for which the orientation of the coordinate system toward the gravitational acceleration is important, all calculations are invariant toward this coordinate system rotation.

3.4. Diapycnal Diffusivities and Richardson Number Dynamics

[26] Stratification and current shear measurements can be combined to estimate the gradient Richardson number Ri:

$$Ri = \frac{N^2}{\left(\frac{\partial u_1}{\partial x_3}\right)^2 + \left(\frac{\partial u_2}{\partial x_3}\right)^2},$$

which describes the dynamic stability of a stratified shear flow [*Miles*, 1961]. Whenever Ri falls below a critical value of $Ri_c \approx 0.25$ (although suggestions in the literature range from 0.2 to 1.0) the formerly parallel shear flow becomes unstable and turbulent mixing occurs. Diapycnal diffusivities K_z can be estimated by considering an equilibrium between shear production of TKE on one side and buoyancy flux and dissipation of TKE on the other side (stationary and homogeneous conditions):

$$K_z = \frac{R_f}{1 - R_f} \frac{\varepsilon}{N^2}$$

where $R_f = -(g\rho^{-1}\ \overline{u_3'\rho'})/(\overline{u_i'u_j'}\frac{\partial \overline{u_i}}{\partial x_j})$ is the flux Richardson number, which was found upon laboratory experiments to have a maximum value of $R_f \approx 0.25$ [*Linden*, 1979]. Time series of the gradient Richardson number, dissipation rates and diapycnal diffusivities for an internal wave event are exemplified in Figure 10. During the calm period, before the internal wave trains were observed at the sampling site (cf. Figure 2c and Figure 4b), Ri fluctuates between 0.1 and 100, whereas it rarely falls below the critical value of $Ri_c \approx 0.25$. With the arrival of the internal wave train, Ri drops and values below Ri_c occur frequently. Simultaneously, the dissipation rate increases by almost four orders of magnitude and the diffusivity K_z increases from $K_z \approx 5{\cdot}10^{-6}$ m^2 s^{-1} during the calm period to peak values of $K_z \approx 5{\cdot}10^{-2}$ m^2 s^{-1}. The frequency distribution of diapycnal diffusivities observed during the entire period of measurements ranges from 10^{-7} to 10^{-2} m^2 s^{-1} with a peak around $K_z \approx 10^{-5}$ m^2 s^{-1} (Figure 11).

4. Discussion and Concluding Remarks

[27] The benthic boundary layer at the depth of the seasonal thermocline is characterized by strong periodic

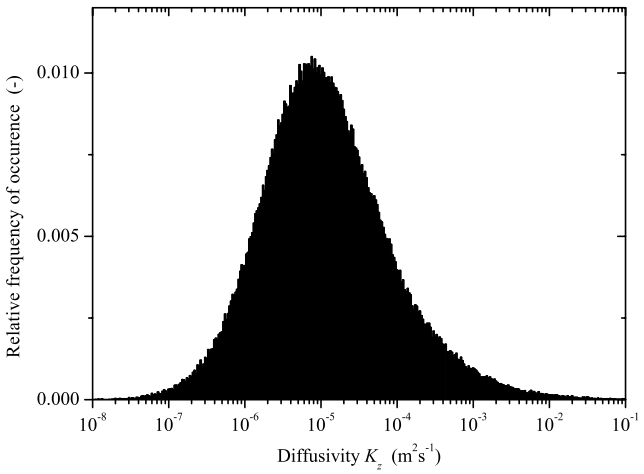

Figure 11. Frequency distribution of $\log_{10}(K_z)$ for the entire data set. The distribution is normalized by the total number of observations.

fluctuations of temperature and current velocity, which are caused by propagating internal waves. The observed periods of these waves in Lake Constance vary between 5 and 20 min and their amplitudes in the open water column are up to 10 m.

[28] The propagation of such high-frequency waves is restricted to the thermocline region between 2 and 30 m depth and shoaling of these waves along the sloping boundaries at this depth causes near-bottom temperature and current velocity fluctuations with amplitudes of up to 10°C and 15 cm s^{-1}, respectively, on temporal scales of the internal wave periods. Power spectral density of temperature fluctuations at the corresponding frequencies is a factor of 6 higher at the boundary than offshore (Figure 3). Although internal wave spectra in lakes are time dependent and, unlike the ocean, a universal (canonical) internal wave spectrum does not exist, this intensification of spectral energy estimated over a rather long time period implies an energy loss to mixing along the boundaries [*Eriksen*, 1982].

[29] Although the occurrence of propagating internal waves is ubiquitous, the observation of trains of large amplitude waves is strongly correlated to the phase of the basin-scale internal Kelvin wave [*Lorke et al.*, 2006]. In accordance with studies in other lakes [*Boegman et al.*, 2003] the high-frequency waves are riding on the crest of a Kelvin wave, suggesting that they are generated by nonlinear steepening of the basin-scale internal wave, as it was demonstrated in laboratory experiments [*Boegman et al.*, 2005b; *Horn et al.*, 2001]. Although it was shown by *Lorke et al.* [2006] that linear internal waves with the observed periods meet the criterion of critical reflection at the study site very closely, the application of the concept of inclined wave propagation in a constant density gradient is rather questionable, given the restricted vertical extension of the thermocline region (Figure 2d).

[30] Whereas the seasonal dynamics of high-frequency internal waves at the same study site was discussed in greater detail by *Lorke et al.* [2006], the present study reveals the dynamics of bottom-boundary layer turbulence by providing a unique long-term data set on dissipation rates of TKE. The dissipation rate estimates are based on acoustic velocity measurements capable of resolving the inertial subrange of turbulent velocity fluctuations, in time (inertial dissipation technique), and in space (structure function method). The structure function method, in particular, allows for dissipation rate estimates on very short sampling intervals, which could be considered as a prerequisite for sampling turbulence in a highly dynamic environment. The comparison with dissipation rates estimated by using the inertial dissipation technique, which involves considerable temporal averaging, however, reveals a reasonable agreement between both methods (cf. Figure 6b), which is also manifested in the almost perfect agreement of the dissipation rate spectra (Figure 7). The peak in the spectral density of the dissipation rates at a period around 4 days, the period of the dominant basin-scale Kelvin wave, provides further evidence for the energy flux path concept outlined above. Since the passage of the Kelvin wave at the sampling site does not provide sufficient spectral power to be detectable in the near-bottom current velocity measurements [*Lorke et al.*, 2006], the peak in the dissipation spectra cannot be attributed to periodic TKE production by current shear associated with the Kelvin wave directly. It can rather be attributed to the saw-tooth like dissipation rate dynamics depicted in Figure 6b, which is caused by packets of high-frequency internal waves riding on the crest of the Kelvin wave passing by the sampling site (cf. Figures 2b and 2c). Dissipation rates within such turbulence bursts can exceed 10^{-4} W·kg^{-1} (Figure 6), which is two orders of magnitude higher than the maximum dissipation rates estimated in the thermocline of Lake Constance away from the boundaries by *Kocsis et al.* [1998]. The statement that the enhanced dissipation rates are the result of wave breaking and not high bottom shear stress is further supported by the vertical profiles of current velocity and dissipation rates (Figure 8), showing that the actual shear layer is compressed to a height of 0.2–0.3 m above the bottom during periods of high dissipation.

[31] Local diapycnal diffusivities can exceed their most frequently observed value of $K_z \approx 10^{-5}$ m^2 s^{-1} by more than three orders of magnitude during such internal wave events. The peak in the frequency distribution of observed diffusivities (Figure 11) is in good agreement with a basin-wide diffusivity of $K_z \approx 3.4 \cdot 10^{-5}$ m^2 s^{-1} traced simultaneously by SF_6 and heat in the thermocline of Lake Constance by *Maiss et al.* [1994]. The frequency distribution, however, is skewed toward higher diffusivities and in order to compare the locally measured diffusivities with the long-term and basin-scale mean provided by tracer measurements, they have to be averaged linearly. The overall arithmetic mean of the nearshore diffusivities of $2 \cdot 10^{-4}$ m^2 s^{-1} is an order of magnitude higher than the tracer-based basin-scale diffusivity estimate and can be regarded as an indicator of enhanced diapycnal mixing along the boundaries at the depth of the seasonal thermocline.

[32] An understanding of the detailed dynamics of small-scale turbulence and mixing, however, seems to be more complicated. A local equilibrium between shear production and dissipation of TKE does not exist, indicating that the turbulence is not homogenous and that transport and divergence of TKE are locally important. This contradicts the assumption of a steady state spectral energy transfer from larger to smaller scales, underlying both methods used for

estimating TKE dissipation rates. The close correspondence between the different dissipation estimates involving rather different scales of temporal and spectral averaging, respectively, suggests that the "patchy" spatial TKE distribution does not consist of coherent structures, e.g., enhanced TKE production further up or further downslope, but is rather statistically distributed. This scenario would lead to reliable dissipation rate estimates via averaging, on one hand, and to a temporal mismatch between local estimates of the Reynolds stress and the corresponding shear profile and hence to a mismatch between the local TKE production and dissipation rate estimates on the other hand. Richardson numbers and diapycnal diffusivities estimated in such a dynamic flow have to be considered as even more critical because their calculation includes the buoyancy frequency, which might not match the local current shear and dissipation rate estimate. Further problems in defining appropriate background profiles of current shear and stratification arise due to overlapping spatial and temporal scales of internal wave motions as the main forcing and current shear and density gradients generated by turbulent eddies. The contribution of the latter must be removed from the background shear and stratification estimate by temporal averaging. Averaging the current shear within an internal wave, however, cannot result in an appropriate shear estimate if the averaging interval exceeds a quarter of the wave period, i.e., 2–5 min.

[33] **Acknowledgments.** I thank H. Hofmann, J. Halder and B. Rosenberg for their help in the field and F. Peeters, S.A. Thorpe, and two anonymous reviewers for helpful comments on earlier manuscripts. This work was financially supported by the German Research Foundation within the framework of the Collaborative Research Center 454 – "The littoral zone of Lake Constance".

References

Appt, J., J. Imberger, and H. Kobus (2004), Basin-scale motion in stratified Upper Lake Constance, *Limnol. Oceanogr.*, *49*(4), 919–933.

Baker, M. A., and C. H. Gibson (1987), Sampling turbulence in the stratified ocean: Statistical consequences of strong intermittency, *J. Phys. Oceanogr.*, *17*, 1817–1836.

Bäuerle, E., D. Ollinger, and J. Ilmberger (1998), Some meteorological, hydrological, and hydrodynamical aspects of Upper Lake Constance, *Arch. Hydrobiol. Spec. Issues Adv. Limnol.*, *53*, 31–83.

Boegman, L., J. Imberger, G. N. Ivey, and J. P. Antenucci (2003), High-frequency internal waves in large stratified lakes, *Limnol. Oceanogr.*, *48*(2), 895–919.

Boegman, L., G. N. Ivey, and J. Imberger (2005a), The degeneration of internal waves in lakes with sloping topography, *Limnol. Oceanogr.*, *50*(5), 1620–1637.

Boegman, L., G. N. Ivey, and J. Imberger (2005b), The energetics of large-scale internal wave degeneration in lakes, *J. Fluid Mech.*, *531*, 159–180.

Dewey, R. K., and G. B. Crawford (1988), Bottom stress estimates from vertical dissipation rate profiles on the continental shelf, *J. Phys. Oceanogr.*, *18*, 1167–1177.

Eriksen, C. C. (1982), Observations of internal wave reflection off sloping boundaries, *J. Geophys. Res.*, *87*(C1), 525–538.

Eriksen, C. C. (1985), Implications of ocean bottom reflection for internal wave spectra and mixing, *J. Phys. Oceanogr.*, *15*, 1145–1156.

Eriksen, C. C. (1998), Internal wave reflection and mixing at Fieberling Guyot, *J. Geophys. Res.*, *103*(C2), 2977–2994.

Gregg, M. C. (1980), Microstructure patches in the thermocline, *J. Phys. Oceanogr.*, *10*, 915–943.

Helfrich, K. R. (1992), Internal solitary wave breaking and run-up on a uniform slope, *J. Fluid Mech.*, *243*, 133–154.

Hondzo, M., and Z. Haider (2004), Boundary mixing in a small stratified lake, *Water Resour. Res.*, *40*, W03101, doi:10.1029/2002WR001851.

Horn, D. A., J. Imberger, and G. N. Ivey (2001), The degeneration of large-scale interfacial gravity waves in lakes, *J. Fluid Mech.*, *434*, 181–207.

Imberger, J. (1998), Flux paths in a stratified lake: A review, in *Physical Processes in Lakes and Oceans*, edited by J. Imberger, pp. 1–18, AGU, Washington, D. C.

Ivey, G. N., and J. Imberger (1991), On the nature of turbulence in a stratified fluid. Part I: The energetics of mixing, *J. Phys. Oceanogr.*, *21*, 650–658.

Ivey, G. N., and R. I. Nokes (1989), Vertical mixing due to the breaking of critical internal waves on sloping boundaries, *J. Fluid Mech.*, *204*, 479–500.

Javam, A., J. Imberger, and S. Armfield (1999), Numerical study of internal wave reflection from sloping boundaries, *J. Fluid Mech.*, *396*, 183–201.

Kocsis, O., B. Mathis, M. Gloor, M. Schurter, and A. Wüest (1998), Enhanced mixing in narrows: A case study at the Mainau sill (Lake Constance), *Aquat. Sci.*, *60*(3), 236–252.

Ledwell, J. R., E. T. Montgomery, K. L. Polzin, L. C. St-Laurent, R. W. Schmitt, and J. M. Toole (2000), Evidence for enhanced mixing over rough topography in the abyssal ocean, *Nature*, *403*, 179–182.

Linden, P. F. (1979), Mixing in stratified fluids, *Geophys. Astrophys. Fluid Dyn.*, *13*, 3–23.

Lorke, A., and A. Wüest (2005), Application of coherent ADCP for turbulence measurements in the bottom boundary layer, *J. Atmos. Oceanic Technol.*, *22*, 1821–1828.

Lorke, A., L. Umlauf, T. Jonas, and A. Wüest (2002), Dynamics of turbulence in low-speed oscillating bottom-boundary layers of stratified basins, *Environ. Fluid Mech.*, *2*, 291–313.

Lorke, A., F. Peeters, and E. Bäuerle (2006), High-frequency internal waves in the littoral zone of a large lake, *Limnol. Oceanogr.*, *51*, 1935–1939.

MacIntyre, S., K. M. Flynn, R. Jellison, and J. R. Romero (1999), Boundary mixing and nutrient fluxes in Mono Lake, California, *Limnol. Oceanogr.*, *44*(3), 512–529.

Maiss, M., J. Ilmberger, and K. O. Münnich (1994), Vertical mixing in Überlingersee (Lake Constance) traced by SF_6 and heat, *Aquat. Sci.*, *56*, 329–347.

McPhee, M. G. (1998), An inertial dissipation method for estimating turbulent flux in buoyancy-driven, convective boundary layers, *J. Geophys. Res.*, *103*(C2), 3249–3255.

Mellor, G. L. (2002), Oscillatory bottom boundary layers, *J. Phys. Oceanogr.*, *32*, 3075–3088.

Miles, J. W. (1961), On the stability of heterogeneous shear flow, *J. Fluid Mech.*, *10*, 496–508.

Moum, J. N., D. R. Caldwell, J. D. Nash, and G. D. Gunderson (2002), Observations of boundary mixing over the continental slope, *J. Phys. Oceanogr.*, *32*, 2113–2130.

Osborn, T. R. (1980), Estimates of the local rate of vertical diffusion from dissipation measurements, *J. Phys. Oceanogr.*, *10*, 83–89.

Rudnick, D. L., T. J. Boyd, R. E. Brainard, G. S. Carter, G. D. Egbert, M. C. Gregg, P. E. Holloway, J. M. Klymak, E. Kunze, C. M. Lee, M. D. Levine, D. S. Luther, J. P. Martin, M. A. Merrifield, J. N. Moum, J. D. Nash, R. Pinkel, L. Rainville, and T. B. Sanford (2003), From tides to mixing along the Hawaiian Ridge, *Science*, *301*, 355–357.

Slinn, D. N., and J. J. Riley (1996), Turbulent mixing in the oceanic boundary layer caused by internal wave reflection from sloping terrain, *Dyn. Atmos. Oceans*, *24*, 51–62.

Stips, A. (2005), Dissipation measurement: theory, in *Marine Turbulence: Theories, Observations, and Models*, edited by H. Baumert, J. H. Simpson, and J. Sündermann, pp. 115–126, Cambridge Univ. Press, Cambridge.

Thorpe, S. A. (1999), 75 + 25 = 99 ± 1, or some of what we still don't know: Wave groups and boundary processes, in *Aha Hulikoa: Dynamics of Oceanic Internal Gravity Waves*, edited by P. Müller and D. Henderson, pp. 129–135, SOEST Special Publication, Honolulu, Hawaii.

Wiles, P. J., T. P. Rippeth, J. H. Simpson, and P. J. Hendricks (2006), A novel technique for measuring the rate of turbulent dissipation in the marine environment, *Geophys. Res. Lett.*, *33*, L21608, doi:10.1029/2006GL027050.

Winters, K. B., P. N. Lombard, J. J. Riley, and E. A. D'Asaro (1995), Available potential energy and mixing in density-stratified fluids, *J. Fluid Mech.*, *289*, 115–128.

Wüest, A., and A. Lorke (2003), Small-scale hydrodynamics in lakes, *Annu. Rev. Fluid Mech.*, *35*, 373–412.

Wunsch, C., and R. Ferrari (2004), Vertical mixing, energy, and the general circulation of the oceans, *Annu. Rev. Fluid Mech.*, *36*, 281–314.

Yamazaki, H., and R. G. Lueck (1990), Why oceanic dissipation rates are not lognormal?, *J. Phys. Oceanogr.*, *20*, 1907–1918.

A. Lorke, Limnological Institute, University of Konstanz, Mainaustrasse 252, D-78464, Konstanz, Germany. (andreas.lorke@uni-konstanz.de)